

Three-dimensional Structure of a Macromolecular Assembly that Regulates Type III Secretion in *Yersinia pestis*

Florian D. Schubot¹, Michael W. Jackson², Kerri J. Penrose¹
Scott Cherry¹, Joseph E. Tropea¹, Gregory V. Plano² and
David S. Waugh^{1*}

¹Macromolecular
Crystallography Laboratory
Center for Cancer Research
National Cancer Institute at
Frederick, P.O. Box B, Frederick
MD 21702-1201, USA

²Department of Microbiology
and Immunology, University of
Miami School of Medicine
Miami, FL 33136, USA

Yersinia pestis, the causative agent of plague, utilizes a type III secretion system (T3SS) to inject effector proteins directly into the cytosol of mammalian cells where they interfere with signal transduction pathways that regulate actin cytoskeleton dynamics and inflammation, thereby enabling the bacterium to avoid engulfment and destruction by macrophages. Type III secretion normally does not occur in the absence of close contact with eukaryotic cells. Negative regulation is mediated in part by a multiprotein complex that has been proposed to act as a physical impediment to type III secretion by blocking the entrance to the secretion apparatus prior to contact with mammalian cells. This complex is composed of YopN, its heterodimeric secretion chaperone SycN–YscB, and TyeA. Here, we report two crystal structures of YopN in complex with its heterodimeric secretion chaperone SycN–YscB and the co-regulatory protein TyeA, respectively. By merging these two overlapping structures, it was possible to construct a credible theoretical model of the YopN–SycN–YscB–TyeA complex. The modeled assembly features the secretion signaling elements of YopN at one end of an elongated structure and the secretion regulating TyeA binding site at the other. A patch of highly conserved residues on the surface of the C-terminal α -helix of TyeA may mediate its interaction with structural components of the secretion apparatus. Conserved arginine residues that reside inside a prominent cavity at the dimer interface of SycN–YscB were mutated in order to investigate whether they play a role in targeting the YopN–chaperone complex to the type III secretion apparatus. One of the mutants exhibited a phenotype that is consistent with this hypothesis.

Published by Elsevier Ltd.

*Corresponding author

Keywords: type III secretion; Tye A; YopN; SycN; YscB

Introduction

Yersinia pestis is the etiologic agent of plague, one of the most devastating diseases in recorded history and a potential instrument of bioterrorism. In *Y. pestis* and many other Gram-negative bacterial pathogens of plants and animals virulence is strictly dependent upon a type III secretion system (T3SS), which serves to direct the translocation of a small

number of proteins, termed effectors, across three membranes from the bacterium into the cytosol of eukaryotic cells.¹ Collectively, these effectors enable the bacteria to disarm the innate immune response of the infected organism by interfering with crucial signal transduction pathways that regulate actin cytoskeleton dynamics and inflammation.

The mechanism underlying the selective targeting of the effectors and other *Yersinia* outer proteins (Yops) for type III secretion has not been clearly established. The secretion signals have been mapped to the N termini of the Yops, but whether they are encoded within their amino acid sequences or within the mRNAs remains controversial.^{2–7} While the N-terminal 10–30 amino acid residues

Abbreviations used: T3SS, type 3 secretion system; Yops, *Yersinia* outer proteins; Sycs, specific Yop chaperones; CBD, chaperone-binding domain.

E-mail address of the corresponding author:
waughd@ncifcrf.gov

(or codons) are essential for the secretion of all Yops, these residues (or codons) bear no obvious sequence similarity to each other, nor do they resemble the signal peptides involved in the more familiar *sec*-dependent or type II secretion pathway. Furthermore, no residues are cleaved from the Yops in transit.

Some proteins that are destined for secretion *via* the T3SS machinery transiently associate with cognate export chaperones called Sycs (specific Yop chaperones). Although Sycs are required for the efficient translocation of their cognate Yops into the host cell, it is not entirely clear what their function is because not all Yops require them. One attractive hypothesis is that the Sycs assist in establishing a hierarchy of secretion for the various effectors, thereby controlling the timing of their delivery into eukaryotic cells.^{8,9} This idea is supported by the observation that the effectors with cognate Sycs appear to be preferentially secreted by the T3SS.^{5,8,10} Alternatively or in addition, Sycs may act to maintain their cognate effectors in a secretion-competent (perhaps partially unfolded) state, prevent their proteolytic degradation in the bacterial cytoplasm, or block premature interactions between them.^{11–15} Moreover, at least in *Salmonella typhimurium*, type III secretion chaperones prevent the improper export of their cognate effectors *via* the flagellar secretion machinery.¹⁶

Several regulatory mechanisms ensure that type III secretion does not occur prior to contact with eukaryotic cells. One of the key regulatory proteins is YopN. YopN also associates with a cognate secretion chaperone, but whereas all other secretion chaperones characterized to date are homodimers,^{10,17} the chaperone for YopN is composed of two distinct polypeptides: SycN and YscB.¹⁸ Strains of *Y. pestis* that lack YopN, SycN, or YscB constitutively secrete other Yops in the absence of eukaryotic cell contact.¹⁹ The same phenotype can also be elicited by deleting the gene encoding a small protein called TyeA,^{20,21} which has been shown to bind to the C terminus of YopN.^{21–23} Accordingly, these four proteins have been proposed to function in concert as negative regulators of the type III secretion process.²² The exact mechanism of action for YopN is not known, but a plausible model proposes that YopN, in association with its chaperone and TyeA, prevents secretion of other Yops into the extracellular milieu by forming a physical blockade within the secretion pore.²² It is thought that the heterodimeric secretion chaperone SycN–YscB initiates YopN into the T3SS, but that YopN cannot be completely secreted while it is bound to TyeA. Upon contact with eukaryotic cells, an unknown signal causes the dissociation of TyeA from the C terminus of YopN, thereby alleviating the molecular plug in the type III secretion apparatus and permitting the secretion of YopN and the other Yops.^{20–22} YopN is translocated by the T3SS into the mammalian cytosol,^{22,24} but it is not

known whether it has an anti-host activity in addition to its proven regulatory function.

Here, we present two crystal structures of YopN in complex with its secretion chaperone SycN–YscB and with the co-regulatory protein TyeA, respectively (Figure 1). This is the first instance in which a type III secretion chaperone has been co-crystallized with a nearly full-length virulence factor. The structural features of this unique heterodimeric chaperone and its interactions with YopN are explored in detail. Structurally conserved residues in a prominent cavity at the dimer interface of SycN–YscB were mutated to investigate their putative role in type III secretion. A credible model of the quaternary assembly that mediates negative regulation of type III secretion in *Y. pestis* was constructed by combining the overlapping SycN–YscB–YopN and YopN–TyeA structures. The molecular architecture of this multiprotein complex suggests how it may function to prevent type III secretion prior to close contact with eukaryotic cells.

Results

Structure of the YopN^{32–277}–SycN–YscB complex

Two orthogonal views of the structure of YopN in complex with its heterodimeric chaperone SycN–YscB are presented in Figure 1(a). The structures of a number of type III secretion chaperones (SycE, SicP, CesT, SigE, Spa15 and SycH) have been reported, including SycE and SycH from *Y. pestis*.^{9,15,25–28} In all cases, homodimers constitute the functional units of the chaperones. A remarkable and unanticipated feature of the present structure is the high degree of structural similarity between the SycN–YscB heterodimer and the homodimeric secretion chaperones (Figure 2(a)). Like its homodimeric counterparts, each monomer in the SycN–YscB complex is composed of three α -helices and a five-stranded antiparallel β -sheet. The α - β - β - β - α - β - α topology positions all three helices on the same face of the β -sheet. In both monomers, residues from helix α -2 and strand β -4 form the dimer interface, resulting in an overall pseudo 2-fold symmetry (Figure 2(b)). The buried surface area between the subunits of the heterodimeric chaperone (ca 2242 Å²) is slightly smaller than the corresponding area in SycE (ca 2638 Å²) but generally comparable to the buried surface area reported for SycH (2200 Å²) and well within the range of 2200–2600 Å² observed for other homodimeric secretion chaperones. Spa15 represents the only outlier in this regard, with a dimer interface of only 1800 Å².²⁷

A closer look, however, reveals striking structural differences that have far reaching consequences for the geometry of the interactions between YopN and its heterodimeric secretion chaperone. In the homodimeric chaperones, helix α -2 is oriented more or

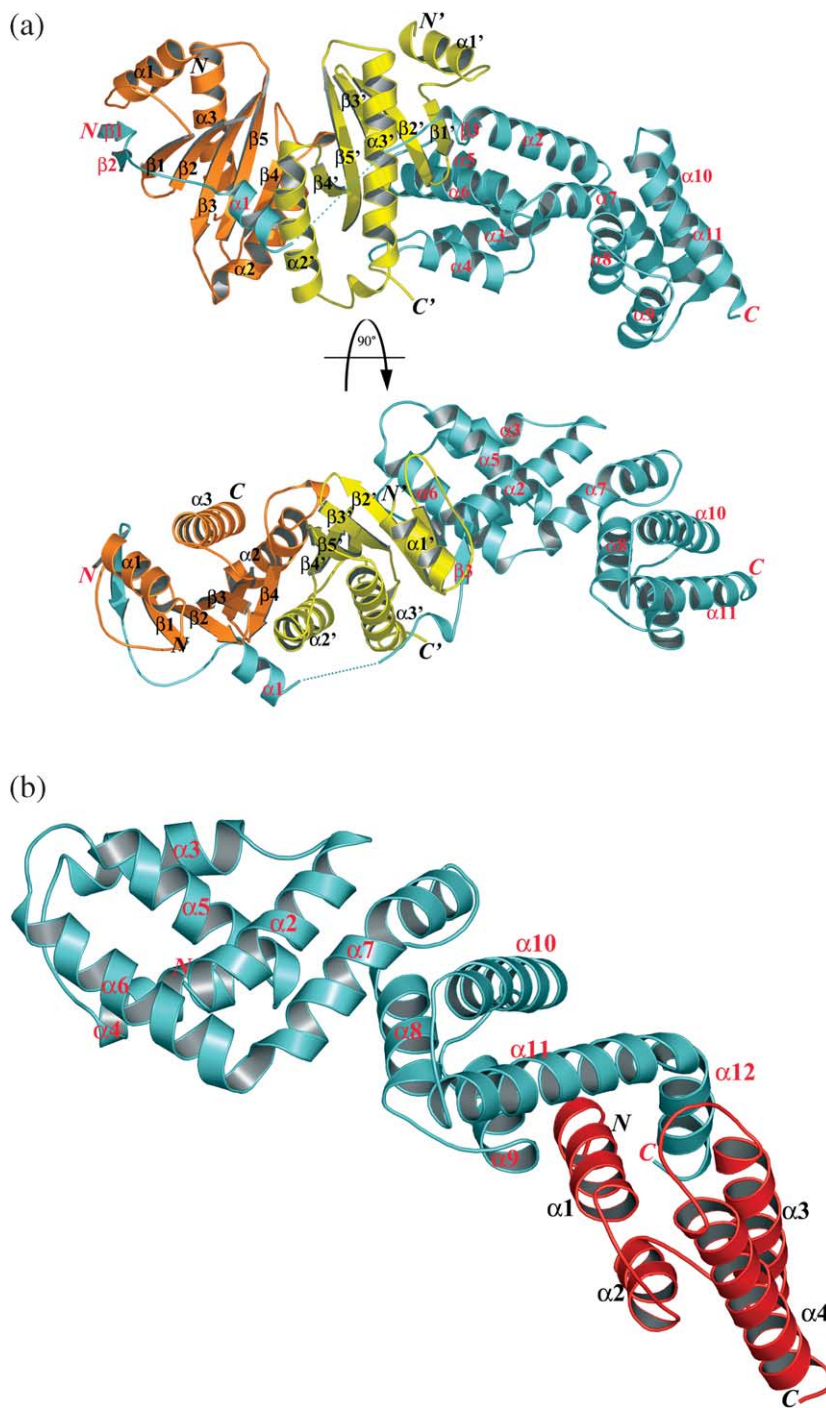


Figure 1. (a) Two orthogonal views showing the ribbon model of the ternary complex between YopN and its heterodimeric secretion chaperone SycN–YscB. YopN, SycN and YscB are represented in cyan, orange and yellow, respectively. The broken line between YopN residues Thr57 and Glu65 denotes the disordered region of the CBD. This Figure was generated by PYMOL⁵¹ (<http://www.pymol.org>). (b) Structure of the YopN¹⁷⁶⁻²⁹³–TyeA complex. YopN and TyeA are depicted in cyan and red, respectively. Helices α -1 and α -3 of TyeA surround helix α -12 of YopN to form the bulk of the intermolecular interface.

less parallel with the dimer interface. The second α -helix of YscB also follows this trend, but this is not the case for SycN. It is here that the structure of SycN–YscB deviates the most from its homodimeric counterparts. The loop connecting elements α -2 and β -3 in SycN is only three residues long as opposed to nine in YscB (and similarly long loops in the other chaperones). This shortened loop causes a significant tilt in the C-terminal part of helix α -2, away from the dimer interface. The tilt in α -2 is complemented by a shift towards the interface of strands β -4 and β -5 in YscB. The net result of these shifts is an asymmetric dimer interface. The

asymmetric nature of the chaperone directly translates into the unique and distinctly asymmetric binding interactions with YopN that dictate the specificity of the interaction.

The chaperone-binding domain (CBD) of YopN is composed of 46 residues that are wrapped around one face of the SycN–YscB structure in the characteristic horseshoe conformation previously observed in the structures of the CBDs from SptP and YopE in complex with their cognate secretion chaperones.^{9,15} As in the SycE–YopE and SicP–SptP complexes, the N terminus of the CBD in YopN (residues 32–43) forms β -strands that interact with

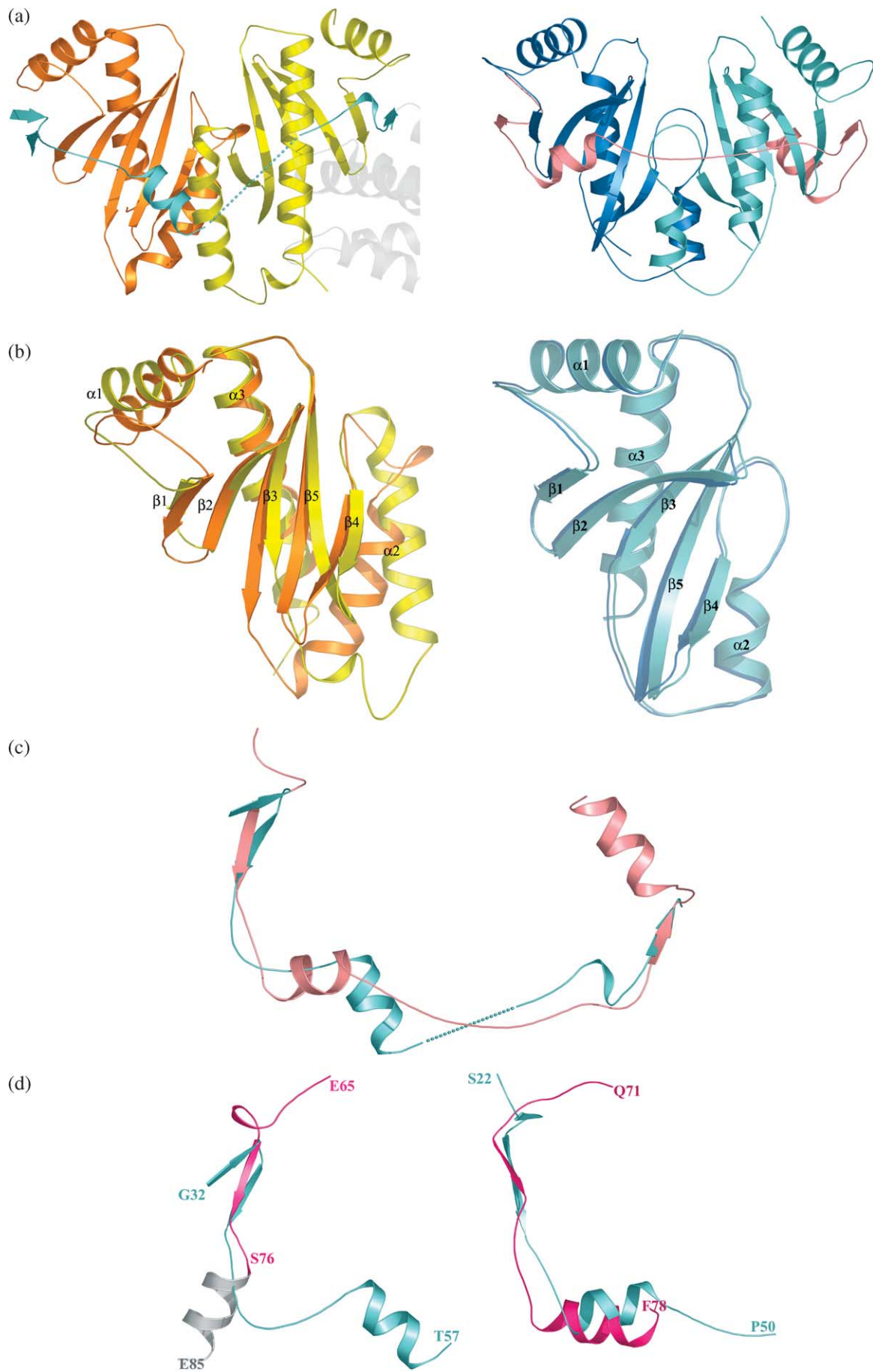


Figure 2 (legend opposite)

the edge of the chaperone (SycN strand β -1), effectively extending its β -sheet. Also conserved is a similar interaction with strand β -1 of YscB on the other side of the chaperone. Linking the conserved elements is a stretch of seven YopN residues (amino acids 58–64) that is disordered in the crystal, suggesting that they do not interact with the chaperone.

Homodimeric T3SS chaperones display perfect 2-fold symmetry, which is also reflected in their effector binding characteristics (i.e. the same areas on each monomer engage in similar interactions with the bound effectors). In SycE and SicP, four major areas of contact, two on each monomer, constitute the effector-binding surfaces.^{9,15} Antiparallel strand–strand interactions are formed between the effectors and the β -1 strands on both edges of the chaperones. SycE and SicP, respectively, bind two helices of YopE and SptP on equivalent hydrophobic patches that are created by the β -sheets on each monomer. The symmetric nature of effector binding is illustrated in Figure 2(d), in which the two adjacent segments of the YopE CBD are structurally aligned.

While all three CBDs follow similar paths along the surfaces of their respective chaperones (Figure 2), only one of the two hydrophobic helix-binding regions conserved between SycE and SicP is present in SycN–YscB. Moreover, the helix-binding region of the latter chaperone features a distinct topology and binds helix α -1 of YopN in an orientation that is quite different from the corresponding helical segments of YopE and SptP in their respective complexes with SycE and SicP (Figure 2(c)). The helix-binding groove in SycN–YscB is located closer to the dimer interface and is comprised of residues from both monomers, including a substantial contribution from helix α -2 of YscB. In contrast to the hydrophobic nature of the helix-binding grooves in SycE and SicP, a combination of hydrophobic and hydrophilic residues from SycN–YscB participate in the interaction with helix α -1 of YopN (Figure 3). Most strikingly, no equivalent helix-binding region exists on the other side of the heterodimeric secretion chaperone, and YopN departs from the chaperone immediately following its interaction with the β -sheet of YscB to form the first of two α -helical domains. For this reason, a smaller surface area is buried at the interface between the CBD of YopN and SycN–YscB

(ca 3596 Å²) than is buried, for instance, in the complex between SycE and the CBD of YopE (ca 4596 Å²).

It should be noted that there are a few additional points of contact between YscB and YopN in the crystal structure of the ternary complex that are not mediated by the CBD of the latter molecule. The significance of these interactions (e.g. a 3 Å hydrogen bond between Ser119 of YopN and Asp53 of YscB) is not clear. However, because the residues comprising the interface between YscB and the adjacent α -helical domain of YopN are not conserved in orthologs from other bacterial pathogens (*Pseudomonas aeruginosa*, *Photobacterium luminescens*, *Aeromonas salmonicida*, and *Vibrio parahaemolyticus*) and residues 1–100 of YopN are sufficient for chaperone binding,²² these contacts are unlikely to be of major importance.

The CBD ends at residue 76, after which YopN folds into two α -helical domains (Figure 1(a)). Residues 95–110 were poorly defined in the electron density map, and therefore only the main-chain atoms could be modeled with confidence. The seemingly rigid boundary between the two α -helical domains of YopN is defined by a slightly kinked helix (α -7), the N terminus of which interacts with α -2 from one domain while its C terminus interacts with helices α -8 and α -10 from the other. The last eight residues of this particular YopN construct (270–277) were not visible in the electron density map.

Structurally conserved arginine residues in SycN–YscB

It has been suggested that type III secretion chaperones may function as supplementary secretion signals that facilitate specific contacts between the effector and components of the secretion apparatus.^{9,16} The recently demonstrated interaction between the chaperone CesT and the putative ATPase EscN, a central component of the T3SS in enteropathogenic *Escherichia coli*, has provided the first direct experimental support for this hypothesis.²⁹ An interaction between a secretion chaperone (FlgN) and a membrane-associated ATPase (FliI) has also been observed in the flagellar secretion/assembly system, which has many features in common with the T3SS.³⁰ The mechanism of dissociation of the chaperone from

Figure 2. (a) Comparison of the SycN–YscB structure with bound CBD of YopN (left) and the SycE–YopE complex (right panel) highlighting the conserved overall fold of the chaperones. (b) Structural alignment of SycN (orange) and YscB (yellow), underlining the structural differences between the two proteins, particularly between strands β -4 and β -5 and the α -2 helices. The latter two structural elements form the dimer interface and are responsible for the asymmetric nature of the chaperone (left panel). The right panel gives the equivalent view for SycE showing the two SycE molecules in different shades of blue and the salmon colored CBD of YopE. (c) Structural alignment of the CBDs of YopE (pink) and YopN (cyan). Conserved are the beta-strands that interact along both sides of the chaperones, but the two helical regions present in the CBD of YopE are either aligned differently (helix 1) or absent in YopN. (d) Structural alignment of two segments from the CBDs of YopN (left) and YopE (right). Following the strand–strand interaction with YscB, YopN folds away from the chaperone into its second domain. The gray helical region beginning at residue 78 can be seen in the image. The binding of YopE to SycE, on the other hand, closely reflects the 2-fold symmetry of the chaperone. The SptP–SicP interactions closely resemble those of the YopE–SycE complex and are therefore not illustrated in the Figure.

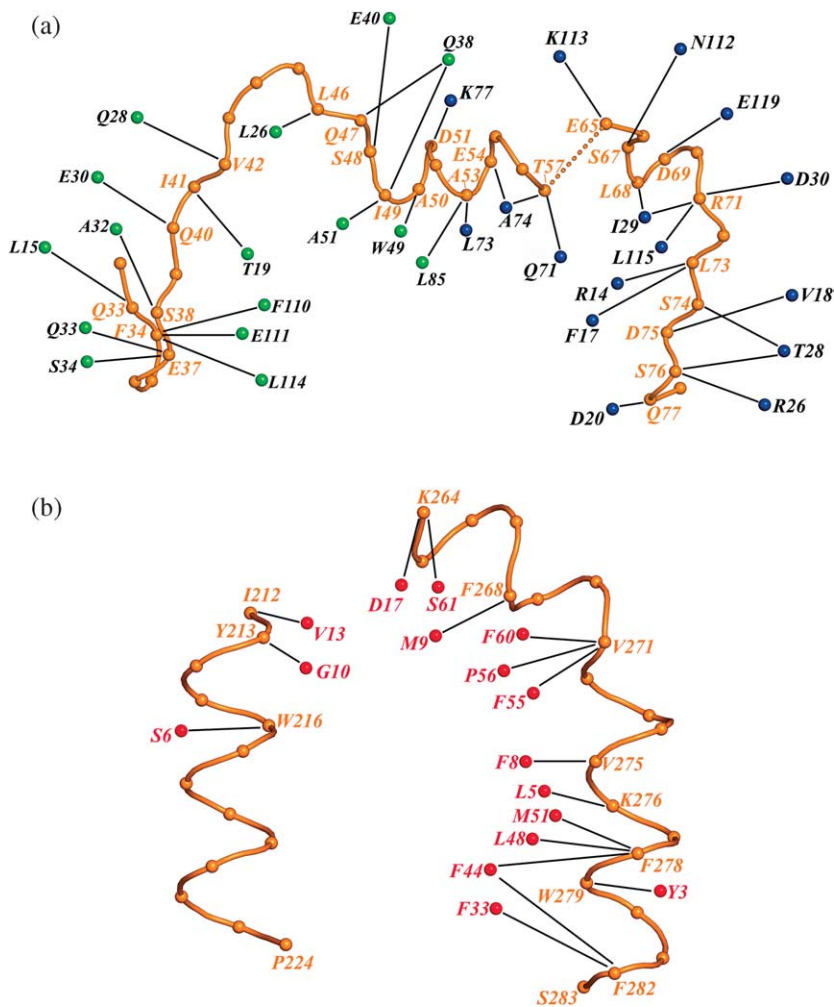


Figure 3. (a) Schematic representation of the hydrophobic (inside the orange colored YopN backbone) and hydrophilic (outside the YopN backbone) contacts between YopN and SycN–YscB. SycN and YscB residues are colored green and blue, respectively. A combination of residues from both SycN and YscB interact with helix α -1 of YopN, in contrast to the homodimeric secretion chaperones, in which the respective helix-binding grooves are formed by residues from a single monomer. (b) Schematic representation of the hydrophobic (inside the orange colored YopN backbone) and hydrophilic (outside the YopN backbone) contacts between the YopN and the TyeA. TyeA atoms are represented as red spheres. Shown here are contacts that are conserved between both of the complexes in the asymmetric unit of the crystal. Striking is the overwhelmingly hydrophobic quality of the interface. The distance cutoff criterion for hydrophilic contacts was set to 3.5 Å, while hydrophobic interactions were considered up to 3.9 Å. Both main-chain and side-chain interactions are included.

the ATPase as well as its release from the seemingly tightly bound effector remain unknown, but ATP hydrolysis likely plays a role in one or both steps.

After SycE^{9,25} and SycH²⁸ SycN–YscB represents the third *Y. pestis* T3SS chaperone for which structural information has become available. Although, as described above, the folds of the three chaperones are very similar, a comparison of their sequences and electrostatic surface properties yielded little insight into their putative role in type III secretion, as their sequences are poorly conserved and charge distributions are quite different. The only conspicuously conserved feature is the presence of two positively charged regions at the bottom of a large cavity that is located at the dimer interface (Figure 4(a)). In the SycE and SycH structures, these patches are respectively formed by the two Arg92 and Arg80 residues from each monomer.^{9,25} The equivalent residues in the structure of the heterodimeric chaperone are Arg81 of SycN and Arg96 of YscB (Figure 4(b)).

Remarkably, residues forming this positively charged area at the heart of the dimer interface are conserved among all recognizable orthologs of SycE, SycH, SycN, and YscB, as well as in the structures of CesT and SigE. Only the cavity of SicP from *S. typhimurium* lacks such residues at its core.

The otherwise divergent nature of the chaperone sequences and the unusual location of the conserved arginine residues deep inside a cavity seem suggestive of a functional role for these residues and possibly the cavity as a whole. Since this region is not involved in effector binding, it may participate in the secretion signaling process by interacting with some component of the T3SS apparatus, possibly the ATPase YscN.

To evaluate the functional significance of the conserved arginine residues in SycN (Arg81) and YscB (Arg96), they were replaced by alanine or aspartic acid residues and then expressed from multicopy plasmids in *Y. pestis* strains lacking wild-type SycN, YscB, or both. Type III secretion was monitored by Western blotting with anti-YopN and anti-YopM antisera in the presence and absence of calcium (Figure 4(c)), which serves as an artificial trigger of secretion in the absence of contact with eukaryotic cells.³¹ Neither of the alanine mutants, either separately or together, had any perceptible effect on the export of YopM or YopN in this assay. This result argues against a direct role for these positively charged side-chains in type III secretion. On the other hand, the charge reversal substitution in SycN (R81D) selectively reduced YopN export and gave rise to a calcium-blind phenotype (i.e. in

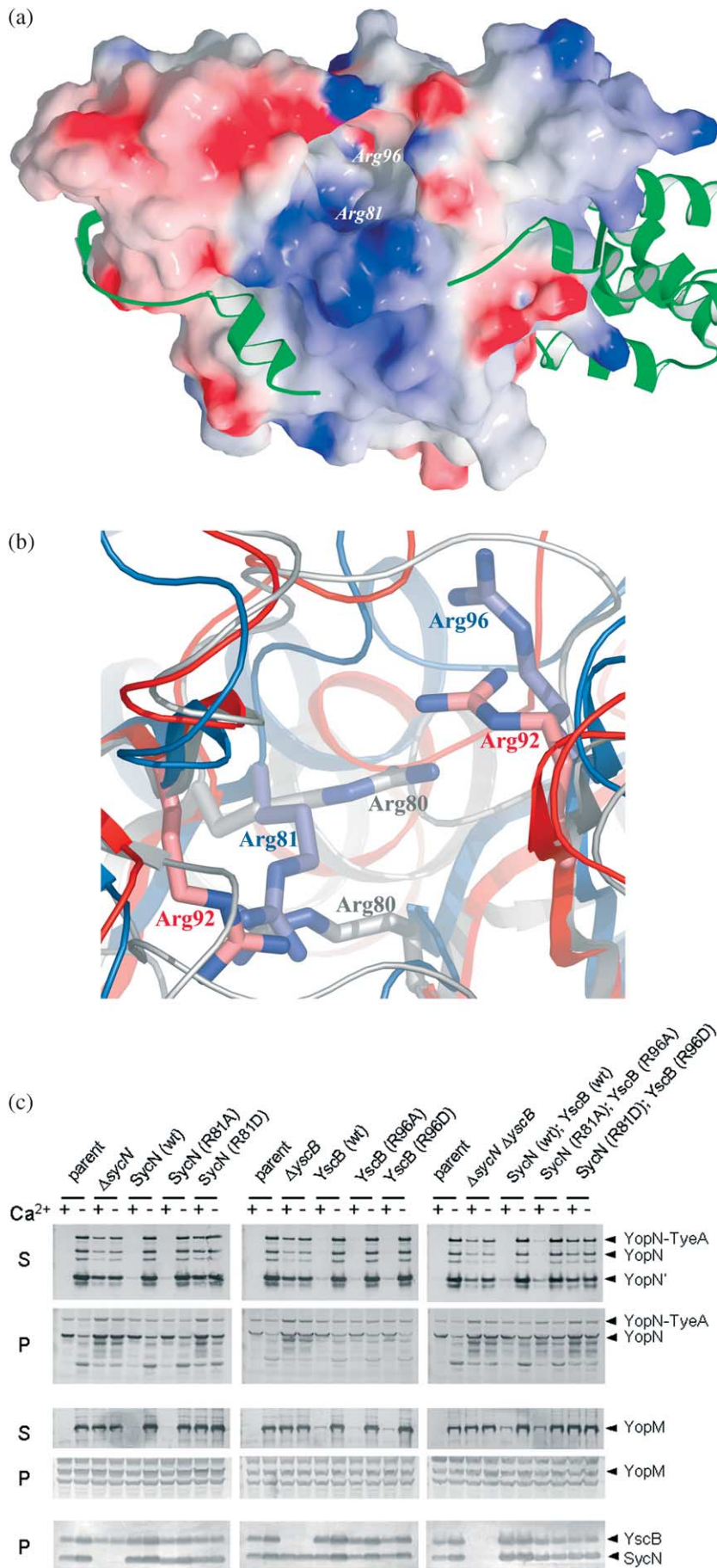


Figure 4. (a) Space-filling model of SycN–YscB showing the distribution of electrostatic potential combined with a cartoon depiction of YopN is aimed at illustrating the positively charged character of the large cavity at the SycN–YscB interface. Labeled are the two arginine residues that create this feature, which is also conserved in other chaperones and might therefore bear functional significance, potentially in the secretion signaling process. This Figure was generated with MOLSCRIPT,⁵² GRASP,⁵³ and Raster3D.⁵⁴ The color scale of electrostatic potential ranged from dark red (–12 kT/e) to dark blue (+12 kT/e). (b) A backbone superposition of SycN–YscB (blue), SycE (red), and SycH (grey) in the vicinity of the cavity at the dimer interface highlights the spatial conservation of Arg92 in SycE, Arg80 in SycH, and Arg96 and Arg81 in YscB and SycN, respectively. (c) Secretion of YopM and YopN by *Y. pestis* strains expressing SycN (R81A), SycN (R81D), YscB (R96A), and YscB (R96D) either alone or in combination. *Y. pestis* KIM5-3001.P40 (parent); KIM5-3001.P46 (Δ sycN) alone and complemented with plasmid pBAD30-SycN [SycN (wt)], pBAD30-SycN(R81A) [SycN (R81A)] or pBAD30-SycN(R81D) [SycN (R81D)]; KIM5-3001.P47 (Δ yscB) alone and complemented with plasmid pBAD18-YscB [YscB (wt)], pBAD18-YscB(R96A) [YscB (R96A)] or pBAD18-YscB(R96D) [YscB (R96D)]; and KIM5-3001.P60 (Δ sycN Δ yscB) alone and complemented with plasmid pairs pBAD30-SycN/pBAD18-YscB [SycN (wt); YscB (wt)], pBAD30-SycN(R81A)/pBAD18-YscB(R96A) [SycN (R81A); YscB (R96A)] or pBAD30-SycN(R81D)/pBAD18-YscB(R96D) [SycN (R81D); YscB (R96D)] were grown in TMH medium containing 0.2% L-arabinose with (+) or without (–) 2.5 mM CaCl₂ for five hours at 37 °C. Volumes of culture supernatant (S) and/or cell pellet (P) fractions corresponding to equal numbers of bacteria were separated by SDS-PAGE, transferred to Immobilon-P membranes, and probed with antisera specific for YopM, YopN, SycN or YscB. The locations of YopN, the YopN–TyeA fusion protein, YopN' (secreted YopN clipped by the Pla protease), YopM, SycN and YscB are shown by arrowheads.

the presence and absence of calcium, with the latter serving as an artificial trigger), indicative of a defect in regulated secretion. These defects do not appear to be caused by destabilization of the SycN(R81D)–YscB–YopN complex, however, because it behaved just like the wild-type ternary complex during protein purification (data not shown). Moreover, none of the mutations altered the expression levels of SycN or YscB in *Y. pestis*. Hence, the phenotype of this mutation suggests that the cavity may somehow be involved in secretion signaling. Curiously, however, the complementary substitution in YscB (R96D) had no discernable effect on calcium-dependent secretion.

Structure of the YopN⁷⁶⁻²⁹³–TyeA complex

The structure of the YopN⁷⁶⁻²⁹³–TyeA complex seamlessly completes the C-terminal domain of YopN (Figure 1(b)). There are two complexes in the asymmetric unit of the crystal. Due to the differing crystal environments, most of residues 95–110, which were disordered in the YopN³²⁻²⁷⁷–SycN–YscB–His₆ complex, fold into a well-ordered helix in one of the two non-equivalent YopN⁷⁶⁻²⁹³–TyeA structures but remain disordered in the other. YopN residues 270–277, also disordered in the ternary complex, are organized into an α -helix in the complex with TyeA. This helix is connected to helix α -11 (residues 249–270) by a two-residue linker, giving this entire segment the appearance of a single helix with a 50° kink between residues 270 and 272. The final ten residues of YopN (284–293) were not visible in either binary complex.

A DALI search³² did not identify any structural homologs of YopN in the Protein Data Bank. Moreover, if one examines the locations of solvent accessible residues that are conserved in orthologs of YopN from other bacterial pathogens, no clear patterns emerge that might indicate what surfaces beyond those involved in TyeA binding might be functionally important; conserved residues are more or less evenly distributed over the surfaces of both domains. The structural uniqueness of YopN provides no insight into a putative functional role it might assume once it has been injected into the host cell, but points away from an enzymatic activity.

The structure of TyeA is composed of two pairs of parallel helices, with a twist of more than 60° between them (Figure 1(b)). Overall, the TyeA molecules in both complexes have well defined structures, although the five C-terminal residues are disordered in one of them. Like YopN, TyeA appears to have a distinct fold; a DALI search³² failed to identify any closely related structures in the PDB. Only eight residues are strictly conserved among distinct orthologs of TyeA (Figure 5(a)). Surprisingly, only one of them is located at the interface between YopN and TyeA. The other seven are clustered together on the C-terminal helix of the protein (Figure 5(b)). This helix faces away from the remainder of the complex, suggesting that TyeA

may utilize it to mediate contacts with structural components of the type III secretion apparatus.

The molecular interface between YopN and TyeA is composed primarily of hydrophobic residues located on four α -helices (Figure 3(b)). The C-terminal helix of YopN (α -12) is sandwiched between the first and third helices of the TyeA molecule. In addition to its interactions with α -12, the N-terminal helix of TyeA forms a number of contacts with YopN helix α -9 (residues 212 to 222). This finding is somewhat curious in view of previous data that indicated residues 248–293 of YopN are sufficient for TyeA binding.²¹ Nevertheless, because these interactions are preserved between the two non-equivalent YopN⁷⁶⁻²⁹³–TyeA complexes in the crystal (RMSD 1.34 Å), we believe they constitute an integral part of the YopN–TyeA interface.

Also noteworthy is the close proximity of the C terminus of YopN and the N terminus of TyeA in the complex (Figure 1(b)). In *Desulfovibrio vulgaris* and *Bordetella bronchiseptica*, YopN and TyeA exist as single polypeptides, and a translational frameshifting event gives rise to the production of a functional YopN–TyeA fusion protein in *Y. pestis* as well.²³ The relative orientation of YopN and TyeA in the complex explains why there are no deleterious structural or functional consequences when the two polypeptides are fused together.

Discussion

Structural insights provided by the unique heterodimeric secretion chaperone SycN–YscB

An interesting observation to emerge from this study concerns the molecular architecture of the heterodimeric type III secretion chaperone SycN–YscB, which exhibits a pseudo 2-fold symmetry that is reminiscent of the homodimeric secretion chaperones. Thus, SycN–YscB does not represent a new structural class of cytosolic export chaperones, but is instead a variation on the same theme. Like the homodimeric chaperones, SycN–YscB binds its partner (YopN) in an extended conformation with some secondary but no tertiary structure. These interactions are far more asymmetric than those that occur between homodimeric chaperones and their cognate effectors because of the intrinsic asymmetry of the heterodimer. In principal, the asymmetry of heterodimeric secretion chaperones should enable them to bind their cognate partners with greater specificity, yet the specificity of the homodimeric chaperones appears to be entirely adequate. In contrast to the genes that encode homodimeric secretion chaperones, which are generally located in close proximity to their cognate Yops, the *yscB* locus is the first gene in a multicistronic operon that predominately encodes essential components of the type III secretion apparatus. Hence, this unusual arrangement may be designed to coordinate the

with the secretion chaperones and that the latter may only play a supplementary role in the process. Indeed, a significant amount of YopN is secreted in the absence of SycN–YscB (Figure 4(c)), making it difficult to distinguish between chaperone-dependent and chaperone-independent secretion. To accomplish this, it may be necessary to engineer a YopN species whose secretion is entirely dependent on the chaperone. This feat was achieved for the SycE–YopE system by constructing a hybrid YopE protein with defective N-terminal secretion signal and a functional SycE binding domain.³³ This approach may work for YopN as well, but will require an in-depth analysis of a variety of mutants.

SycN–YscB is the first type III secretion chaperone to be co-crystallized with a large portion of its cognate binding partner. As the structure of the YopN^{76–293}–TyeA complex subsequently revealed, chaperone binding did not produce long-range conformational effects on YopN beyond its CBD. The vast majority of the contacts between SycN/YscB and YopN are mediated by the CBD of the latter molecule. The remaining contacts between the helical domains of YopN and its chaperone are not conserved in orthologous proteins, suggesting that they are unlikely to be biologically significant. Thus, the structure confirms the notion that Yops have a modular architecture in which the N-terminal secretion signals and CBDs are structurally and functionally independent from the remainder of the proteins.

Structural basis of the YopN–TyeA regulatory switch

The very C terminus of YopN (residues 278–293) is readily cleaved by thermolysin in the absence of TyeA, suggesting that, under these circumstances, it may either be disordered or loosely attached to the remainder of the protein.³⁴ In the structure of the YopN^{76–293}–TyeA complex, however, the bond between YopN residues 277 and 278 is located well within the C-terminal α -helix, giving no indication that this site would be highly susceptible to proteolysis. Interestingly, the ¹H–¹⁵N heteronuclear single quantum coherence NMR spectrum of TyeA exhibits only a few cross peaks (data not shown). Since TyeA behaves as a monomer during size exclusion chromatography, thus excluding aggregation as the cause for the observed spectrum, this finding suggests that by itself TyeA does not assume a clearly defined tertiary structure in solution. Therefore, the association of TyeA with the C terminus of YopN is likely accompanied by conformational changes in both polypeptides that create order out of disorder. The resulting structure then serves as an impediment to type III secretion. Such a mechanism could serve to ensure that TyeA does not bind to the secretion apparatus in the absence of YopN.

Yet, by itself, the formation of a complex between YopN and TyeA is insufficient to block type III secretion, as evidenced by the fact that YopN is

secreted in the absence of its chaperone but in the presence of TyeA (Figure 4(c)). Moreover, the YopN–TyeA fusion protein is also secreted in the absence of the chaperone (Figure 4(c)). This indicates that YopN must interact simultaneously with both SycN–YscB and TyeA in order to suppress type III secretion.

The root mean square deviation (RMSD) between the conformation of YopN in its ternary complex with SycN–YscB and in its binary complex with TyeA is a mere 1 Å, which is less than the difference between two YopN^{76–293} molecules in the same crystal (1.3 Å). Consequently, it was possible to build a model of the quaternary YopN–SycN–YscB–TyeA complex as it is very likely to exist in the cytosol of *Y. pestis* (Figure 6). The resulting molecular assembly has a decidedly non-globular appearance. It also appears to be fairly rigid, as all molecular and domain interfaces are sizable and formed by inflexible structural elements. The shape of the quaternary complex is consistent with a scenario in which the N-terminal secretion signal of YopN, in conjunction with its secretion chaperone SycN–YscB, initiates the molecule into the secretion channel while TyeA, located at the opposite end of the multiprotein complex, mediates its arrest, perhaps by using its conserved C-terminal helix to interact reversibly with one or more structural components of the secretion apparatus. We propose that the central domain of YopN serves as a molecular yardstick to facilitate contacts between opposite ends of the quaternary complex with equidistant binding sites on the secretion apparatus, both of which are required to properly engage the molecular stopper that negatively regulates type III secretion in *Y. pestis*. However, the mechanism by which contact with eukaryotic cells or the removal of calcium from the culture medium induces the dissociation of YopN–TyeA from the secretion apparatus remains to be elucidated.

Materials and Methods

Expression, purification and crystallization of the YopN^{32–277}–SycN–YscB–His₆ complex

Initial attempts to overproduce and purify YopN, SycN, or YscB individually were hampered by their poor solubility. However, co-expression of full-length YopN (residues 1–293) with SycN and YscB–His₆ in *E. coli* yielded a stable complex that could readily be purified to homogeneity but would not crystallize. When the ternary complex was subjected to limited proteolysis with thermolysin, a stable digestion product corresponding to residues 32–277 of YopN was generated.³⁴ On the basis of this observation, a new vector was constructed to co-express residues 32–277 of YopN with SycN and YscB–His₆.

Co-expression, purification, and crystallization of the YopN^{32–277}–SycN–YscB–His₆ complex has been described elsewhere in detail.³⁴ Briefly, a multicistronic expression vector encoding a truncated form of YopN (residues 32 to 277), SycN, and YscB–His₆ was assembled by Gateway multisite recombinational cloning, using the destination

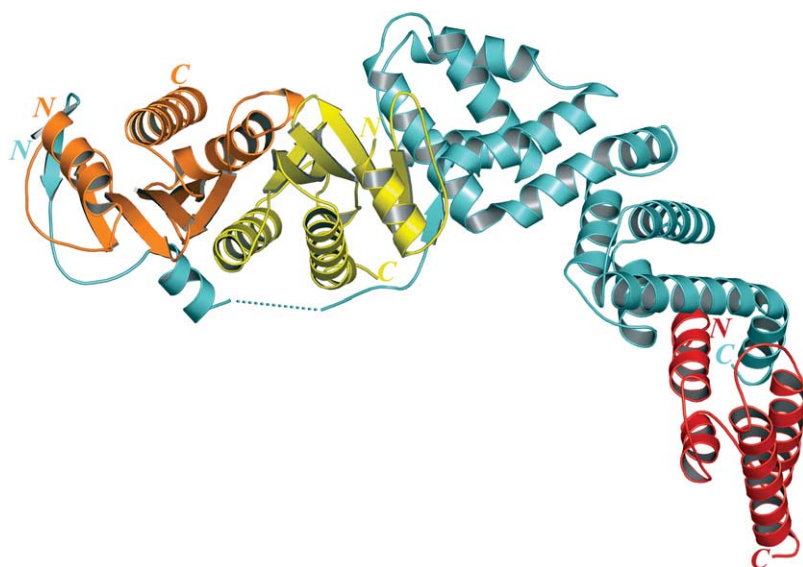


Figure 6. A model of the YopN–SycN–YscB–TyeA complex constructed by merging the two overlapping crystal structures. The RMSD of only 1 Å between the YopN molecules in the two structures allowed the construction of the model, which in all likelihood depicts the assembly as it exists in the *Y. pestis* cytoplasm. Noteworthy are the seeming rigidity of the structure and the spatial separation of secretion targeting and secretion regulating elements.

vector pDEST-42 (Invitrogen, Carlsbad, CA). Identical ribosome binding sites were added in the appropriate positions upstream of the open reading frames by PCR. The recombinant proteins were expressed in *E. coli* BL21(DE3) CodonPlus RIL cells (Stratagene, La Jolla, CA), which were induced at mid-log phase with 1 mM IPTG for four hours. The selenomethionine-substituted ternary complex was produced using the saturation of the methionine biosynthetic pathway protocol.³⁵ The ternary complex was purified by immobilized metal affinity chromatography and gel filtration. The sample was subsequently subjected to reductive methylation³⁴ and screened for crystallization conditions. Optimized conditions, consisting of 0.1 M Hepes (pH 6.8), 0.4 M magnesium chloride, 22% (w/v) PEG 3350, and protein complex at 10 mg/ml in 25 mM Tris–HCl (pH 7.4), 0.15 M sodium chloride, yielded the tetragonal crystals used for the structure solution.

Expression, purification and crystallization of the YopN^{76–293}–TyeA complex

The structure of YopN^{32–277} in complex with SycN–YscB–His₆ delineated the boundaries of its CBD. On the basis of this information, a different fragment of YopN, lacking the N-terminal secretion signal and the CBD but extending all the way to its natural C terminus (YopN^{76–293}), was co-expressed with TyeA in *E. coli* from a multicistronic vector constructed by Gateway multisite recombinational cloning. A TEV protease recognition site and the appropriate att recombination sites (attB1 and attB3) were added to the TyeA open reading frame (ORF) during PCR and then the amplicon was recombined into pDONR208 (Invitrogen). Similarly, a ribosome binding site and the appropriate att recombination sites (attB3 and attB2) were added to the YopN ORF during PCR and then this amplicon was recombined into pDONR209 (Invitrogen). The nucleotide sequences of the two ORFs were verified, after which they were recombined in tandem into the destination vector pDEST–HisMBP³⁶ to create the multicistronic expression vector pKP1563, which was designed to produce TyeA as a fusion to the C terminus of an N-terminally His-tagged *E. coli* maltose-binding protein (MBP) along with YopN^{76–293} as a free-standing polypeptide.

Single colonies of *E. coli* BL21(DE3) CodonPlus RIL

cells (Stratagene, La Jolla, CA) containing pKP1563 were used to inoculate 100 ml of Luria broth supplemented with glucose at 2 g l^{–1}, 100 µg ml^{–1} ampicillin, and 30 µg ml^{–1} chloramphenicol. The culture was grown with shaking (225 rpm) to saturation overnight at 37 °C and then diluted 66-fold into six liters of fresh medium. When the cells reached early log phase ($A_{600\text{ nm}} = 0.5$), the temperature was reduced to 30 °C and isopropyl-β-D-thiogalacto-pyranoside (IPTG) was added to a final concentration of 1 mM. Four hours later, the cells were recovered by centrifugation at 5000g for 15 minutes. The cell paste was resuspended in 400 ml of buffer A (50 mM Hepes (pH 7.6), 150 mM NaCl, 25 mM imidazole) along with four tablets of Complete[®] EDTA-free protease inhibitor cocktail (Roche Molecular Biochemicals, Indianapolis, IN). The cells were lysed with an APV Gaulin model G1000 homogenizer at 10,000 psi and centrifuged at 30,000g for 30 minutes at 4 °C. The supernatant was filtered through a 0.45 µm polyethersulfone membrane and then applied to a 25 ml Ni-NTA Superflow affinity column (Qiagen, Valencia, CA) equilibrated with buffer A. The column was washed with five column volumes of buffer A and then eluted with a linear gradient from 25 mM to 250 mM imidazole. The His–MBP–TyeA–YopN^{76–293} complex was then digested with His-tagged TEV(S219V) protease³⁷ overnight, using 1 mg of protease for every 100 mg of fusion protein. The sample was subsequently diluted sixfold in 50 mM Hepes (pH 7.6), 150 mM NaCl in order to reduce the imidazole concentration. Next, it was once again applied to a 25 ml Ni-NTA Superflow affinity column (Qiagen) equilibrated with buffer A. The flow-through fractions now contained the cleaved YopN^{76–293}–TyeA complex. The sample was concentrated to about 10 mg ml^{–1} using an Amicon YM10 membrane (Millipore, Billerica, MA) and applied to a 26/60 HiLoad Superdex 75 prep grade column (Amersham Biosciences, Piscataway, NJ) equilibrated with buffer B (25 mM Hepes (pH 7.4), 150 mM NaCl). The peak fractions containing the ternary complex were pooled and concentrated to 15 mg ml^{–1}. Aliquots were flash-frozen with liquid nitrogen and stored at –80 °C until use. The final product was judged to be >95% pure by sodium dodecyl sulfate–polyacrylamide gel electrophoresis (data not shown). The molecular masses were confirmed by electrospray mass spectrometry.

Although crystals of the YopN^{76–293}–TyeA complex

were obtained quickly, their diffraction properties were poor ($>7 \text{ \AA}$). Therefore, the pure YopN⁷⁶⁻²⁹³–TyeA complex was subjected to reductive methylation as described³⁴ and subsequently applied to a 26/60 HiLoad Superdex 75 prep grade column equilibrated with 25 mM Tris–HCl (pH 7.4), 150 mM NaCl. After concentrating the purified YopN⁷⁶⁻²⁹³–TyeA complex to 15 mg ml^{-1} , screening for crystallization conditions was conducted. Optimized conditions, consisting of 0.1 M Caps (pH 10.5), 2 M ammonium sulfate, 0.2 M lithium sulfate and protein complex at 15 mg ml^{-1} in 25 mM Tris–HCl (pH 7.4), 0.15 M NaCl, yielded the orthorhombic crystals used for the structure solution.

X-ray data collection

Crystals of the YopN³²⁻²⁷⁷–SycN–YscB–His₆ complex were mounted in a loop after cryo-soaking in 0.1 M Hepes

(pH 6.8), 0.4 M MgCl₂, 22% PEG 3350, 5% glycerol and subsequently flash-frozen in liquid nitrogen. All datasets used for the structure solution were collected at the SER-CAT beamline 22-ID (Advanced Photon Source, Argonne National Laboratory). Data processing was carried out with the HKL2000 program suite.³⁸ Details of data collection and processing for all data sets are provided in Table 1.

Crystals of the YopN⁷⁶⁻²⁹³–TyeA complex were mounted in a loop after cryo-soaking in 0.1 M Caps (pH 10.5), 2 M ammonium sulfate, 0.2 M lithium sulfate, 20% glycerol, and subsequently flash-frozen in liquid nitrogen. The first dataset was collected from a single crystal using a MAR-345 image plate mounted on a Rigaku X-ray generator, yielding diffraction data up to a resolution of 2.7 Å. A second dataset was collected from the same crystal at the SER-CAT beamline 22-ID, where the diffraction limit was about 2.2 Å. However, the low-resolution data ($>4 \text{ \AA}$) were of relatively poor

Table 1. Crystallization and refinement statistics

A. Data collection statistics				
	YopN ³²⁻²⁷⁷ –SycN–YscB–His ₆			YopN ⁷⁶⁻²⁹³ –TyeA
	Native	Se-Met	AuCl ₄ - derivative	
Molecules/a.u.	1			2
Wavelength (Å)	1.0668		1.00	1.54/1.00
Space group	<i>P</i> 4 ₁	<i>P</i> 4 ₁	<i>P</i> 4 ₁	<i>P</i> 2 ₁ 2 ₁ 2
Unit cell parameters (Å)	<i>a</i> = <i>b</i> = 60.72, <i>c</i> = 140.42	<i>a</i> = <i>b</i> = 60.94, <i>c</i> = 140.92	<i>a</i> = <i>b</i> = 60.71, <i>c</i> = 140.42	<i>a</i> = 82.17 <i>b</i> = 170.72 <i>c</i> = 55.58
Resolution (Å)	50–1.84	20–2.0	20–2.5	20–2.2
Total reflections	915,853	530,445	385,183	207,442
Unique reflections	43,586	29,364	15,920	40,229
Completeness (%) ^a	99.2 (98.4)	84.8 (16.3)	90.4 (91.6)	99.3 (98.7)
Average <i>I</i> /σ	26.8 (4.13)	26.5 (1.6)	24.7 (2.6)	29.3 (3.1)
<i>R</i> _{merge} (%) ^b	4.9 (31.6)	7.2 (41.0)	8.0 (45.4)	8.7 (45)
Twin fraction (%)	17	32	0	–
B. Phasing statistics (23–1.9 Å)				
	YopN ³²⁻²⁷⁷ –SycN–YscB–His ₆			
	Native	Se-Met	AuCl ₄ -	
Number of heavy atom sites	–	5	4	
Mean FOM of phasing (SOLVE)	0.20			
Overall FOM of phasing (RESOLVE)	0.52			
<i>R</i> for <i>F</i> _C versus <i>F</i> _P (%)	29.7			
C. Refinement statistics				
Model	YopN ³²⁻²⁷⁷ –SycN–YscB–His ₆		YopN ⁷⁶⁻²⁹³ –TyeA	
Resolution range (Å)	23–1.84		20–2.2	
<i>R</i> (%) ^c	19.0		18.8	
<i>R</i> _{free} (%) ^d	23.2		25.0	
Root mean square deviation bond lengths (Å)	0.018		0.022	
Root mean square deviation angles (deg.)	1.65		1.95	
Temperature factor (Å ²)	20.6		41.8	
Number of protein atoms	7557		4699	
Number of solvent molecules	227		180	
Ramachandran analysis (%)				
Most favored	93.6		91.9	
Allowed	6.4		8.1	
Disallowed	0		0	

^a The values in parentheses relate to the highest resolution shell.

^b $R_{\text{merge}} = \sum |I| - I / \sum I$, where *I* is the observed intensity, and \bar{I} is the average intensity obtained from multiple observations of symmetry-related reflections after rejections.

^c $R = \sum ||F_o| - |F_c|| / \sum |F_o|$, where *F*_o and *F*_c are the observed and calculated structure factors, respectively.

^d *R*_{free} defined by Merritt & Bacon.⁵⁵

quality, possibly due to scattering from the mount pin. Therefore, the low-resolution data (20–3.5 Å) collected in-house were merged with the unaffected data (4–2.2 Å) collected at the synchrotron and the resulting composite dataset was used for structure solution. The data collection and processing statistics are provided in Table 1.

Structure solution and refinement

An evaluation of the diffraction data from the YopN^{32–277}–SycN–YscB–His₆ crystals revealed varying degrees of merohedral twinning, with twin-fractions ranging from 1% to 42% as estimated by the Merohedral Twinning Server†. The best native crystal had a reasonable twin fraction of about 17% and diffracted X-rays to a resolution of 1.84 Å, while none of the screened selenomethionine-substituted crystals had a twin-fraction of less than 30%. Furthermore, these crystals were quite susceptible to radiation damage, making it difficult to obtain a complete high quality MAD dataset from a single crystal. Consequently, the phases obtained from MAD experiments were insufficient to solve the structure. To gain additional phase information, an AuCl₄[–] derivative was generated from crystals of the native complex by soaking them for one day in cryo solution containing 1 mM KAuCl₄. Fortunately, one of the derivatized crystals was not twinned.

The dataset from the native crystal and the peak dataset from the selenomethionine derivative were “detwinned” using the program DETWIN,³⁹ and, together with the AuCl₄[–] derivative, analyzed in SOLVE.⁴⁰ The resulting MIRAS phases were directly channeled into RESOLVE.⁴¹ The initial 1.9 Å map and partial backbone trace created by RESOLVE were of excellent quality, exhibiting clear protein/solvent boundaries and recognizable features of protein secondary structure. After density modification, nearly the entire backbone and most of the side-chains could be traced with the molecular modeling program O.⁴² The model was refined with REFMAC,⁴³ followed by manual adjustment against SIGMAA³⁹ weighted difference Fourier maps. After several rounds of manual adjustment and refinement, 227 water molecules were added to the structure using ARP/wARP⁴⁴ in combination with REFMAC.

The structure of the YopN^{76–293}–TyeA complex was solved by molecular replacement, using the model of YopN^{76–269} as a template in MOLREP.³⁹ The obtained solution, which contained two molecules of YopN^{76–269}, was used to generate initial phases that were greatly improved after applying density modification as implemented by RESOLVE. The density modified map allowed fitting of almost the entire backbone of both TyeA molecules and most of the side-chains in the molecular modeling program O.⁴² After several rounds of manual adjustment and refinement, 180 water molecules were added to the structure using ARP/wARP⁴⁴ in combination with REFMAC.

Model quality was assessed with PROCHECK.⁴⁵ All non-glycine residues in both crystal structures resided either in the most favorable or in the allowed regions of the Ramachandran plot and the overall geometry was better than average when compared to structures solved at the same resolution. Model refinement statistics are given in Table 1.

Y. pestis strains and growth conditions

Y. pestis strains used in this study are Pgm- and thus avirulent from peripheral routes of infection.⁴⁶ *Y. pestis* KIM5-3001.P40 (pCD1 *sycE yopE::km yopJ*), KIM5-3001.P46 (pCD1 *sycE yopE::km yopJ sycN*), KIM5-3001.P47 (pCD1 *sycE yopE::km yopJ yscB*) and KIM5-3001.P60 (pCD1 *sycE yopE::km yopJ sycN yscB*) were used for complementation studies and Yop secretion assays.²⁴ *Y. pestis* KIM5-3001.P60 (pCD1 *sycE yopE::km yopJ sycN yscB*) was constructed *via* allelic exchange using *Y. pestis* KIM5-3001.P46 and plasmid pUK4134.P3 as described.¹⁸ These strains and derivatives of these strains were grown in the presence and absence of 2.5 mM CaCl₂ in the defined medium TMH as described.⁴⁷

Site-directed mutagenesis of *sycN* and *yscB*

The *sycN* and *yscB* genes were amplified *via* PCR from plasmid pCD1 of *Y. pestis* KIM5 using 5' primers that contain a KpnI restriction site and 3' primers that contain an XbaI restriction site. After digestion with KpnI and XbaI the *sycN* and *yscB* products were inserted into KpnI and XbaI-digested plasmid pBAD30 or pBAD18Cm⁴⁸ generating plasmids pBAD30-SycN and pBAD18-YscB. Site-directed mutagenesis of the *sycN* codon encoding Arg81 (CGA) of pBAD30-SycN and the *yscB* codon encoding Arg96 (CGT) of pBAD18-YscB to Ala (GCA) or Asp (GAC) was accomplished using the PCR-ligation-PCR technique.⁴⁹

Measurement of YopM and YopN secretion

Y. pestis strains were grown in TMH medium for five hours at 37 °C in the presence or absence of 2.5 mM CaCl₂. Cultures were centrifuged at 5000g for ten minutes to pellet bacteria. Culture supernatants containing the secreted Yops were precipitated with 10% trichloroacetic acid (TCA). Cell pellet and culture supernatant fractions were resuspended in SDS-PAGE solubilization buffer. Volumes of cellular fractions corresponding to equal numbers of bacteria were analyzed by SDS-PAGE and immunoblot analysis with antisera specific for YopM, YopN, SycN and YscB.

Protein Data Bank atomic coordinates

The atomic coordinates and structure factors for the YopN–SycN–YscB and YopN–TyeA structures have been deposited in the RCSB Protein Data Bank (PDB)⁵⁰ with accession codes 1XKP and 1XL3, respectively.

Acknowledgements

We thank Karen Routzahn and Howard Peters for their early contributions to this work and the SBL Biophysics Core Resource (US National Cancer Institute at Frederick) for the use of the electrospray mass spectrometer. We also thank Dr Zbigniew Dauter for his valuable advice on the merohedral twinning problem. X-ray diffraction data were collected at the Southeast Regional Collaborative Access Team (SER-CAT) 22-ID beamline at the Advanced Photon Source, Argonne National

† <http://www.doe-mpi.ucla.edu/Services/Twinning/>

Laboratory. Supporting institutions may be found at www.ser-cat.org/members.html. Use of the Advanced Photon Source was supported by the US Department of Energy, Office of Science, Office of Basic Energy Sciences, under contract no. W-31-109-Eng-38.

References

- Cornelis, G. R. (2002). The *Yersinia* Ysc-Yop “type III” weaponry. *Nature Rev. Mol. Cell. Biol.* **3**, 742–752.
- Lloyd, S. A., Norman, M., Rosqvist, R. & Wolf-Watz, H. (2001). *Yersinia* YopE is targeted for type III secretion by N-terminal, not mRNA, signals. *Mol. Microbiol.* **39**, 520–531.
- Ramamurthi, K. S. & Schneewind, O. (2003). *Yersinia* yopQ mRNA encodes a bipartite type III secretion signal in the first 15 codons. *Mol. Microbiol.* **50**, 1189–1198.
- Ramamurthi, K. S. & Schneewind, O. (2002). *Yersinia enterocolitica* type III secretion: mutational analysis of the yopQ secretion signal. *J. Bacteriol.* **184**, 3321–3328.
- Anderson, D. M. & Schneewind, O. (1999). *Yersinia enterocolitica* type III secretion: an mRNA signal that couples translation and secretion of YopQ. *Mol. Microbiol.* **31**, 1139–1148.
- Anderson, D. M. & Schneewind, O. (1997). A mRNA signal for the type III secretion of Yop proteins by *Yersinia enterocolitica*. *Science*, **278**, 1140–1143.
- Goss, J. W., Sorg, J. A., Ramamurthi, K. S., Ton-That, H. & Schneewind, O. (2004). The secretion signal of YopN, a regulatory protein of the *Yersinia enterocolitica* type III secretion pathway. *J. Bacteriol.* **186**, 6320–6324.
- Boyd, A. P., Lambermont, I. & Cornelis, G. R. (2000). Competition between the Yops of *Yersinia enterocolitica* for delivery into eukaryotic cells: role of the SycE chaperone binding domain of YopE. *J. Bacteriol.* **182**, 4811–4821.
- Birtalan, S. C., Phillips, R. M. & Ghosh, P. (2002). Three-dimensional secretion signals in chaperone-effector complexes of bacterial pathogens. *Mol. Cell*, **9**, 971–980.
- Feldman, M. F. & Cornelis, G. R. (2003). The multi-talented type III chaperones: all you can do with 15 kDa. *FEMS Microbiol. Letters*, **219**, 151–158.
- Menard, R., Sansonetti, P., Parsot, C. & Vasselon, T. (1994). Extracellular association and cytoplasmic partitioning of the IpaB and IpaC invasins of *S. flexneri*. *Cell*, **79**, 515–525.
- Neyt, C. & Cornelis, G. R. (1999). Role of SycD, the chaperone of the *Yersinia* Yop translocators YopB and YopD. *Mol. Microbiol.* **31**, 143–156.
- Holmstrom, A., Olsson, J., Cherepanov, P., Maier, E., Nordfelth, R., Pettersson, J. *et al.* (2001). LcrV is a channel size-determining component of the Yop effector translocon of *Yersinia*. *Mol. Microbiol.* **39**, 620–632.
- Frithz-Lindsten, E., Rosqvist, R., Johansson, L. & Forsberg, A. (1995). The chaperone-like protein YerA of *Yersinia pseudotuberculosis* stabilizes YopE in the cytoplasm but is dispensible for targeting to the secretion loci. *Mol. Microbiol.* **16**, 635–647.
- Stebbins, C. E. & Galan, J. E. (2001). Maintenance of an unfolded polypeptide by a cognate chaperone in bacterial type III secretion. *Nature*, **414**, 77–81.
- Lee, S. H. & Galan, J. E. (2004). Salmonella type III secretion-associated chaperones confer secretion-pathway specificity. *Mol. Microbiol.* **51**, 483–495.
- Parsot, C., Hamiaux, C. & Page, A. L. (2003). The various and varying roles of specific chaperones in type III secretion systems. *Curr. Opin. Microbiol.* **6**, 7–14.
- Day, J. B. & Plano, G. V. (1998). A complex composed of SycN and YscB functions as a specific chaperone for YopN in *Yersinia pestis*. *Mol. Microbiol.* **30**, 777–788.
- Forsberg, A., Viitanen, A. M., Skurnik, M. & Wolf-Watz, H. (1991). The surface-located YopN protein is involved in calcium signal transduction in *Yersinia pseudotuberculosis*. *Mol. Microbiol.* **5**, 977–986.
- Cheng, L. W. & Schneewind, O. (2000). *Yersinia enterocolitica* TyeA, an intracellular regulator of the type III machinery, is required for specific targeting of YopE, YopH, YopM, and YopN into the cytosol of eukaryotic cells. *J. Bacteriol.* **182**, 3183–3190.
- Iriarte, M., Sory, M. P., Boland, A., Boyd, A. P., Mills, S. D., Lambermont, I. & Cornelis, G. R. (1998). TyeA, a protein involved in control of Yop release and in translocation of *Yersinia* Yop effectors. *EMBO J.* **17**, 1907–1918.
- Cheng, L. W., Kay, O. & Schneewind, O. (2001). Regulated secretion of YopN by the type III machinery of *Yersinia enterocolitica*. *J. Bacteriol.* **183**, 5293–5301.
- Ferracci, F., Day, J. B., Ezelle, H. J. & Plano, G. V. (2004). Expression of a functional secreted YopN-TyeA hybrid protein in *Yersinia pestis* is the result of a +1 translational frameshift event. *J. Bacteriol.* **186**, 5160–5166.
- Day, J. B., Ferracci, F. & Plano, G. V. (2003). Translocation of YopE and YopN into eukaryotic cells by *Yersinia pestis* yopN, tyeA, sycN, yscB and lcrG deletion mutants measured using a phosphorylatable peptide tag and phosphospecific antibodies. *Mol. Microbiol.* **47**, 807–823.
- Evdokimov, A. G., Tropea, J. E., Routzahn, K. M. & Waugh, D. S. (2002). Three-dimensional structure of the type III secretion chaperone SycE from *Yersinia pestis*. *Acta Crystallog. sect. D*, **58**, 398–406.
- Luo, Y., Bertero, M. G., Frey, E. A., Pfuetzner, R. A., Wenk, M. R., Creagh, L. *et al.* (2001). Structural and biochemical characterization of the type III secretion chaperones CesT and SigE. *Nature Struct. Biol.* **8**, 1031–1036.
- van Eerde, A., Hamiaux, C., Perez, J., Parsot, C. & Dijkstra, B. W. (2004). Structure of Spa15, a type III secretion chaperone from *Shigella flexneri* with broad specificity. *EMBO Rep.* **5**, 477–483.
- Phan, J., Tropea, J. E. & Waugh, D. S. (2004). Structure of the *Yersinia pestis* type III secretion chaperone SycH in complex with a stable fragment of YscM2. *Acta Crystallog. sect. D*, **60**, 1591–1599.
- Gauthier, A. & Finlay, B. B. (2003). Translocated intimin receptor and its chaperone interact with ATPase of the type III secretion apparatus of enteropathogenic *Escherichia coli*. *J. Bacteriol.* **185**, 6747–6755.
- Thomas, J., Stafford, G. P. & Hughes, C. (2004). Docking of cytosolic chaperone-substrate complexes at the membrane ATPase during flagellar type III protein export. *Proc. Natl Acad. Sci. USA*, **101**, 3945–3950.
- Michiels, T., Wattiau, P., Brasseur, R., Ruyschaert, J. M. & Cornelis, G. (1990). Secretion of Yop proteins by *Yersinia*. *Infect. Immun.* **58**, 2840–2849.

32. Holm, L. & Sander, C. (1995). Dali: a network tool for protein structure comparison. *Trends Biochem. Sci.* **20**, 478–480.
33. Cheng, L. W., Anderson, D. M. & Schneewind, O. (1997). Two independent type III secretion mechanisms for YopE in *Yersinia enterocolitica*. *Mol. Microbiol.* **24**, 757–765.
34. Schubot, F. D. & Waugh, D. S. (2004). A pivotal role for reductive methylation in the *de novo* crystallization of a ternary complex composed of *Yersinia pestis* virulence factors YopN, SycN and YscB. *Acta Crystallog. sect. D*, **60**, 1981–1986.
35. Doublet, S. (1997). Preparation of selenomethionyl proteins for phase determination. *Methods Enzymol.* **276**, 523–530.
36. Tropea, J. E., Cherry, S., Nallamsetty, S., Bignon, C. & Waugh, D. S. (2005). A generic method for the production of recombinant proteins in *Escherichia coli* using a dual His6-MBP affinity tag. *Methods Mol. Biol.* In the press.
37. Kapust, R. B., Tozser, J., Fox, J. D., Anderson, D. E., Cherry, S., Copeland, T. D. *et al.* (2001). Tobacco etch virus protease: mechanism of autolysis and rational design of stable mutants with wild-type catalytic proficiency. *Protein Eng.* **14**, 993–1000.
38. Otwinowski, Z. M. W. (1997). HKL2000. *Methods Enzymol.* **276**, 307–326.
39. Collaborative Computational Project Number 4. (1994). The CCP4 suite: programs for protein crystallography. *Acta Crystallog. sect. D*, **50**, 760–763.
40. Terwilliger, T. C. & Berendzen, J. (1999). Automated MAD and MIR structure solution. *Acta Crystallog. sect. D*, **55**, 849–861.
41. Terwilliger, T. C. (2000). Maximum-likelihood density modification. *Acta Crystallog. sect. D*, **56**, 965–972.
42. Jones, T. A., Zou, J.-Y., Cowan, S. W. & Kjeldgaard, M. (1991). Improved methods for building protein models in electron density maps and the location of errors in these models. *Acta Crystallog. sect. A*, **47**, 110–119.
43. Murshudov, G. N., Vagin, A. A. & Dodson, E. J. (1997). Refinement of macromolecular structures by the maximum-likelihood method. *Acta Crystallog. sect. D*, **53**, 240–255.
44. Perrakis, A., Morris, R. & Lamzin, V. S. (1999). Automated protein model building combined with iterative structure refinement. *Nature Struct. Biol.* **6**, 458–463.
45. Laskowski, R. A., MacArthur, M. W., Moss, D. S. & Thornton, J. M. (1993). PROCHECK: a program to check the stereochemical quality of protein structures. *J. Appl. Crystallog.* **26**, 283–291.
46. Une, T. & Brubaker, R. R. (1984). *In vivo* comparison of avirulent Vwa- and Pgm- or Pstr phenotypes of yersiniae. *Infect. Immun.* **43**, 895–900.
47. Plano, G. V., Barve, S. S. & Straley, S. C. (1991). LcrD, a membrane-bound regulator of the *Yersinia pestis* low-calcium response. *J. Bacteriol.* **173**, 7293–7303.
48. Guzman, L. M., Belin, D., Carson, M. J. & Beckwith, J. (1995). Tight regulation, modulation, and high-level expression by vectors containing the arabinose PBAD promoter. *J. Bacteriol.* **177**, 4121–4130.
49. Ali, S. A. & Steinkasserer, A. (1995). PCR-ligation-PCR mutagenesis: a protocol for creating gene fusions and mutations. *Biotechniques*, **18**, 746–750.
50. Abola, E. E., Bernstein, F. C., Bryant, S. H., Koetzl, T. F. & Weng, J. (1987). Protein Data Bank. In *Crystallographic Databases—Information Content, Software Systems, Scientific Applications* (Allen, F. H., Bergerhoff, G. & Sievers, R., eds), pp. 107–132, Data Commission of the International Union of Crystallography, Bonn.
51. DeLano, W. L. (2001). The PyMOL Molecular Graphics System. DeLano Scientific LLC, San Carlos, CA, USA.
52. Esnouf, R. M. (1997). An extensively modified version of MolScript that includes greatly enhanced coloring capabilities. *J. Mol. Graph. Model.* **15**, 132–134.
53. Nicholls, A. (1992). *GRASP: Graphical Representation and Analysis of Surface Properties*, Department of Biochemistry and Molecular Biophysics, Columbia University, New York, NY.
54. Merritt, E. A. & Bacon, D. J. (1997). Raster3D photorealistic molecular graphics. *Methods Enzymol.* **277**, 505–524.
55. Gouet, P., Courcelle, E., Stuart, D. I. & Metoz, F. (1999). ESPript: analysis of multiple sequence alignments in PostScript. *Bioinformatics*, **15**, 305–308.

Edited by I. Wilson

(Received 20 October 2004; received in revised form 14 December 2004; accepted 16 December 2004)